Available online at www.sciencedirect.com
SCIENCE DIRECT
ELSEVIER
Journal of Contaminant Hydrology 82 (2006) 99–117
JOURNAL OF Contaminant Hydrology
www.elsevier.com/locate/jconhyd

Concentration dependent transport of colloids in saturated porous media

Scott A. Bradford [a,*], Mehdi Bettahar [b]

[a] George E. Brown, Jr., Salinity Laboratory, USDA, ARS, 450 W. Big Springs Road, Riverside CA 92507-4617, United States
[b] Parsons, 100 West Walnut Street, Pasadena, CA 91124, United States

Received 30 July 2003; received in revised form 31 August 2005; accepted 9 September 2005
Available online 14 November 2005

Abstract

A series of column experiments was undertaken to explore the influence of colloid input concentration (2, 1, 0.5, and 0.25 times a reference concentration), colloid size (negatively charged 3.2 and 1.0 μm carboxyl latex), and sand grain size (360, 240, and 150 μm quartz sands) on transport and deposition. A similar mass of stable mono-dispersed colloids was added to each column. For a given input concentration, decreasing the sand size and increasing the colloid size resulted in increased mass retention in the sand near the column inlet and lower relative concentrations in the effluent. For a given sand and colloid, increasing the input concentration produced less deposition and higher mass recovery in the effluent, especially for coarser sands and smaller colloids. Results of a time dependent attachment (blocking) and detachment model were not consistent with this behavior because the simulations predicted much less retention near the column inlet and a decreasing number of favorable attachment sites (mass of deposited colloids) with increasing input concentration in a given system (colloid and sand). A time dependent straining model (filling of straining sites) provided a better description of the effluent and deposition data, but still could not account for the observed concentration dependent mass recovery. Alternatively, the straining model was refined to include a liberation term that assumed that straining was hindered at higher concentrations (collision frequencies) due to repulsive colloid (aqueous phase)–colloid (strained) interactions. Simulations that included straining, liberation, attachment, and detachment significantly improved the description of the experimental data.
Published by Elsevier B.V.

Keywords: Colloid; Transport; Concentration; Straining; Attachment; Blocking; Liberation

* Corresponding author. Tel.: +1 951 369 4857; fax: +1 951 342 4963.
E-mail address: sbradford@ussl.ars.usda.gov (S.A. Bradford).

0169-7722/$ - see front matter. Published by Elsevier B.V.
doi:10.1016/j.jconhyd.2005.09.006

1. Introduction

A wide variety of inorganic, organic, and microbiological colloids can be found in the subsurface environment (McCarthy and Zacchara, 1989). These colloid particles can be released into sand solution and groundwater through a variety of hydrologic, geochemical, and microbiological processes (Nyhan et al., 1985; Gschwend and Reynolds, 1987; McCarthy and Zacchara, 1989; Ryan and Gschwend, 1990; Ouyang et al., 1996). Many environmental contaminants occur as colloids (pathogenic microorganisms) or are associated with colloids (heavy metals, radionuclides, pesticides, polycyclic aromatic hydrocarbons, etc.) (Ouyang et al., 1996; de Jonge et al., 2004). Also, injection of specific bacteria into the subsurface has been proposed as a means to accelerate the bioremediation of contaminants (Deshpande and Shonnard, 1999; Rockhold et al., 2004). Hence, knowledge of the processes and factors that control colloid transport and fate is required to accurately assess contaminant potential and extent, and to design efficient remediation strategies.

Colloid attachment, the removal of particle mass from solution via collision with and fixation to the porous media, is typically assumed to be the primary mechanism controlling colloid retention in porous media. Attachment is dependent on particle–particle, particle–solvent, and particle–porous media interactions (Elimelech and O'Melia, 1990), as well as sedimentation and interception (Logan et al., 1995). The kinetics of particle attachment are controlled by the rate of transport to solid surfaces and subsequent fixation to these surfaces. According to traditional first-order attachment theory, colloid removal by a porous medium decreases exponentially with depth. An optimum particle size for transport in a given aqueous–porous medium system is also predicted (Tobiason and O'Melia, 1988).

Colloid particles in soil solution may vary widely in concentration, typically ranging from 10^8 to 10^{17} particles per liter (Kim, 1991). Concentration and time dependent attachment coefficients have been reported in the literature (Tan et al., 1994; Lindqvist et al., 1994; Johnson and Elimelech, 1995; Liu et al., 1995; Rijnaarts et al., 1996; Camesano and Logan, 1998; Camesano et al., 1999; Brown et al., 2002). Time dependent attachment coefficients occur as a result of differences in the attachment behavior of colloids on clean porous media and on media already containing attached colloids. Diminished attachment occurs when favorable attachment sites become filled (blocking). Conversely, enhanced attachment may occur when attached particles serve as favorable sites for subsequent colloid attachment (ripening). Liu et al. (1995) found that higher colloid concentrations produced a more rapid filling of favorable attachment sites than lower colloid concentrations. Similarly, Tan et al. (1994) found that bacterial transport through porous media was enhanced at higher cell concentrations. Blocking was proposed as a possible explanation for this behavior.

A second mechanism of colloid retention is straining. Straining is the trapping of colloid particles in down-gradient pore throats that are too small to allow particle passage (McDowell-Boyer et al., 1986). Hence, colloid transport may occur in the larger pores, while colloid retention will occur at pore throats and grain junctions that are below some critical size. Bradford et al. (2002) found in packed column experiments that the peak effluent concentration decreased and the retained mass of colloids increased with increasing size of colloids and decreasing median grain size of the porous media. The majority of the colloid mass was deposited near the column inlet, and the spatial distribution was not exponential. These observations were attributed to colloid straining. Bradford et al. (2003) employed an irreversible, first-order, depth dependent straining coefficient to accurately describe the observed deposition behavior. Other researchers have recently recognized straining as a

potentially important mechanism for colloid deposition (Tufenkji et al., 2004; Redman et al., 2004; Foppen et al., 2005).

Foppen et al. (2005) demonstrated that filling of straining sites by *Escherichia coli* was concentration dependent. The theoretical volume of straining sites for a given colloid and porous medium can be calculated from geometric considerations (Herzig et al., 1970) or measured pore-size distribution information (using capillary pressure–saturation data and Laplace's equation). For a given volume of straining sites, a fixed number of colloids is required to fill these sites. The rate of filling of these sites is dependent on the concentration of the colloids in suspension; e.g., higher colloid concentrations fill straining sites more rapidly than low concentrations.

This manuscript reports on research investigating the role of colloid input concentration on transport and deposition. Special attention has been given to concentration dependent attachment (blocking) and straining (filling) mechanisms of deposition. Little research attention as been given to these topics in the literature, especially concentration dependent straining. Since straining is a strong function of colloid and porous medium size (Bradford et al., 2003), column experiments were conducted over a range of colloid and porous medium sizes, as well as input concentrations. The colloid mass was kept at a similar level in these experiments by adjusting the input concentration and the pulse duration. Accurate identification of deposition mechanisms requires knowledge of both colloid effluent and deposition data (Tufenkji et al., 2003). Colloid transport and deposition were therefore assessed by measuring temporal changes in the effluent concentration and the final spatial distribution of retained colloids. Previous concentration dependent colloid transport studies that have appeared in the literature (Tan et al., 1994; Liu et al., 1995; Foppen et al., 2005) have only considered effluent data (no spatial distribution data). The colloid transport data were described and analyzed using a transport model that accounts for advective, dispersive, and diffusive colloid fluxes, and two-site kinetic deposition. One deposition site accounts for state-of-the-art time dependent attachment according to Langmuirian (Deshpande and Shonnard, 1999) and random sequential adsorption (Johnson and Elimelech, 1995) approaches and first-order detachment. The second deposition site includes novel formulations for time dependent straining and liberation.

1.1. Theory

A generalized form for colloid attachment/detachment models can be written as:

$$\frac{\partial(\rho_b S_{att})}{\partial t} = \theta_w k_{att} \psi_{att} C - \rho_b k_{det} S_{att}. \quad (1)$$

Here C [N L^{-3}; N and L denote number and length, respectively] is the colloid concentration in the aqueous phase, t is time [T; denotes time], ρ_b [M L^{-3}; M denotes mass] is the bulk density of the porous medium, S_{att} [N M^{-1}] is the solid phase concentration of attached colloids, θ_w is the volumetric water content [–], k_{att} [T^{-1}] is the first order colloid attachment coefficient, k_{det} [T^{-1}] is the first order colloid detachment coefficient, and ψ_{att} [–] is a dimensionless colloid attachment function. When ψ_{att} equals 1, clean bed attachment is assumed and the concentration of retained colloids in the porous medium decreases exponentially with depth. The value of ψ_{att} becomes a function of S_{att} to account for colloid blocking, with ψ_{att} decreasing with increasing S_{att}. The value of ψ_{att} is a linear function of S_{att} ($\psi_{att} = 1 - S_{att}/S_{att}^{max}$; where S_{att}^{max} [N M^{-1}] is the maximum solid phase concentration of attached colloids) according to the Langmuirian approach (Deshpande and Shonnard, 1999). In contrast, the random sequential adsorption (RSA) approach employs a ψ_{att} that is a nonlinear function of S_{att} (Johnson and Elimelech, 1995).

Straining is modeled similar to the procedure outlined by Bradford et al. (2003). A colloid liberation expression is also included below to account for repulsive colloid (aqueous phase)–colloid (strained) interactions. The mass balance equation for strained colloids is given as:

$$\frac{\partial(\rho_b S_{str})}{\partial t} = \theta_w k_{str} \psi_{str} C - \theta_w k_{lib} S_{str} C \quad (2)$$

where k_{str} [T^{-1}] is the straining coefficient, k_{lib} [M^{-1} T^{-1}] is the colloid liberation coefficient, ψ_{str} [–] is a dimensionless colloid straining function, and S_{str} [N^{-1}] is the solid phase concentration of strained colloids. The first term on the right hand side of Eq. (2) accounts for colloid straining. The second term accounts for colloid liberation. Retention of strained colloids is hypothesized to be hindered at greater collision frequencies (higher concentrations) due to repulsive colloid (aqueous phase)–colloid (strained) interactions (dependent on the colloid surface chemistry and aqueous chemistry). The frequency of collisions is assumed to be proportional to the colloid concentration in solution (Logan et al., 1995) and the amount retained on the solid phase. Additional justification for this modeling approach will be provided in the Results and discussion section of the manuscript.

The value of ψ_{str} in Eq. (2) is modeled as a function of distance and S_{str} as:

$$\psi_{str} = \left(1 - \frac{S_{str}}{S_{str}^{max}}\right) * \left(\frac{d_{50} + z}{d_{50}}\right)^{-\beta} \quad (3)$$

where z [L] is the distance from the column inlet, S_{str}^{max} [N_c M^{-1}] is the maximum solid phase concentration of strained colloids, and β [–] is a parameter that controls the shape of the (power law) spatial distribution. The first term on the right hand side of Eq. (3) accounts for filling of straining sites in a manner similar to the Langmuirian blocking approach (e.g., Deshpande and Shonnard, 1999). The remaining term (Bradford et al., 2003) assumes that colloid deposition by straining occurs primarily at the column inlet (power law distribution), because the flow field is not yet fully established and colloids therefore have increased accessibility to small pore spaces. The apparent number of small dead-end pores is hypothesized to decrease with increasing distance since size exclusion and/or limited advection and transverse dispersivity tend to keep mobile colloids within the larger networks, thus bypassing smaller pores. Bradford et al. (2003) found that the value of $\beta = 0.432$ gave a good description of the spatial distribution of retained colloids when significant straining occurred. For the remainder of this manuscript β will therefore be fixed to this value.

The HYDRUS-1D computer code (Simunek et al., 1998; Bradford et al., 2003) was modified in this work to account for time dependent colloid attachment (blocking) according to Langmuirian and RSA approaches. The time dependent straining and colloid liberation model discussed above was also implemented. HYDRUS-1D simulates water, heat, and multiple solute movement in one-dimensional variably saturated porous media. The code is coupled to a nonlinear least squares optimization routine based upon the Marquardt–Levenberg algorithm (Marquardt, 1963) to facilitate the estimation of colloid transport parameters from experimental data. Values of the hydrodynamic dispersivity utilized in the simulations presented in this manuscript were taken from Bradford et al. (2003) for the same colloids and porous media.

2. Materials and methods

Many of the experimental materials, procedures and protocols employed herein were described by Bradford et al. (2002). Only a brief discussion of this information is provided

below. Yellow-green fluorescent latex microspheres (Interfacial Dynamics Company, Portland, OR 97224) were used as model colloid particles in the experimental studies (excitation at 490 nm, and emission at 515 nm). Two size diameters of colloid particles (d_c), 1.0 and 3.2 μm, were employed. These microspheres had carboxyl surface functional groups grafted onto latex particle surfaces by the manufacturer to create a negatively charged hydrophobic colloid surface with a particle density of 1.055 g cm^{-3} (provided by the manufacturer) and an air–water contact angle of 115.2° (measured on a lawn of colloids with a Tantec Contact Angle Meter, Tantec Inc., Schaumburg, IL 60193). Specific physical and chemical characteristics for the 1.0 μm particles include: surface charge density of 27 μC cm^{-3} (provided by manufacturer) and zeta potential of $^{-}$83.5 mV (measured with a Zetasizer 3000, Malvern Instruments, Inc., Southborough, MA 01772). In contrast, the 3.2 μm particles had a surface charge density of 11.9 μC cm^{-3} and a zeta potential of $^{-}$85.5 mV. Experiments were designed to examine the concentration dependent transport behavior of a fixed mass of colloids. Four different input concentration (C_i) levels were utilized: $2*C_r$, $1*C_r$, $0.5*C_r$, and $0.25*C_r$, where C_r is the reference concentration equal to 3.86×10^{10} N l^{-1} and 1.18×10^{9} N l^{-1} for the 1.0 and 3.2 μm colloids, respectively. The colloid pulse duration for the $2*C_r$, C_r, $0.5*C_r$, and $0.25*C_r$ systems was equal to $0.5*t_o$, t_o, $2*t_o$, and $4*t_o$, respectively; where t_o is equal to approximately 75 min. The input concentrations, reference concentrations, and pulse durations were selected to provide each column with an equal colloid mass (approximately 3.28 mg) for a given Darcy velocity (approximately 0.1 cm min^{-1}). Following the addition of colloids to the influent, approximately 380 ml of eluant were flushed through the sand.

The colloids and aqueous phase chemistry (pH, ionic strength, and composition) of the tracer, resident, and eluant solutions utilized in the column experiments was chosen to create a stabilized mono-dispersed suspension of the selected colloids. The initial resident and eluant solutions consisted of 0.001 M NaCl with its pH buffered to 6.98 using $NaHCO_3$ (5×10^{-5} M). The colloid-conservative tracer solution consisted of 0.001 M NaBr with pH buffered to 6.73 using $NaHCO_3$ (5×10^{-5} M) and the previously indicated initial colloid concentration. The aqueous solvent for all experimental solutions consisted of deaired (boiled) deionized water. The uniformity of the colloid size distribution in this suspension was verified with a Horiba LA 930 (Horiba Instruments Inc., Irvine, CA 92614) laser scattering particle size and distribution analyzer, indicating that repulsive colloid–colloid interactions occurred for the selected experimental conditions.

Aquifer material used for the column experiments consisted of various sieve sizes of Ottawa (quartz) sand (U.S. Silica, Ottawa, IL 61350). The Ottawa sands will be designated herein as: 3550, MIX, and 70110. These porous media were selected to encompass a range in sand grain size distribution characteristics. Specific properties of the 3550, MIX, and 70110 sands, include: median grain size (d_{50}) of 0.36, 0.24, and 0.15 mm; and uniformity index (d_{60}/d_{10}; here x% of the mass is finer than d_x) of 1.88, 3.06, and 2.25, respectively.

Aluminum columns (10 cm long and 5 cm inside diameter) or Kontes Chromaflex 2 chromatography columns (Kimble/Kontes, Vineland, NJ 08360) made of borosilicate glass (15 cm long and 4.8 cm inside diameter equipped with an adjustable flow adapter at the top) were used in the transport studies. The columns were wet packed with the various porous media. Table 1 provides porosity (ϵ) values (Danielson and Sutherland, 1986) and column lengths for each experimental column. The colloid tracer suspension or eluant solution was pumped upward through the vertically oriented columns at a steady-rate. Effluent samples were collected over the course of each column experiment, and the concentrations of colloids and bromide were measured using a Turner Quantech Fluorometer (Barnstead/Thermolyne, Dubuque, IA 52004-9910) and an Orion 720a pH/ISE meter (Orion Research Inc., Beverly, MA 01915-9846), respectively. The

Table 1
Column properties (column length, L; porosity, ε; and Darcy water velocity, q_w) and the recovered effluent (M_E), sand (M_S), and the total colloid mass fraction (MB_T)

Sand type	C_i/C_r	d_c (μm)	q_w (cm min^{-1})	ε	L (cm)	M_E	M_S	MB_T
3550	2.00	1.00	0.09	0.31	10.00	0.87	0.27	1.14
3550	1.00	1.00	0.10	0.34	12.67	0.87	0.10	0.97
3550	0.50	1.00	0.12	0.27	10.00	0.49	0.36	0.85
3550	0.25	1.00	0.10	0.31	10.00	0.35	0.52	0.87
3550	2.00	3.20	0.12	0.30	10.00	0.41	0.83	1.24
3550	1.00	3.20	0.10	0.34	12.77	0.34	0.73	1.07
3550	0.50	3.20	0.09	0.31	10.00	0.08	1.22	1.30
3550	0.25	3.20	0.08	0.31	10.00	0.06	1.08	1.14
MIX	2.00	1.00	0.13	0.31	10.00	0.81	0.34	1.15
MIX	1.00	1.00	0.11	0.33	12.46	0.84	0.18	1.02
MIX	0.50	1.00	0.14	0.26	10.00	0.35	0.49	0.84
MIX	0.25	1.00	0.11	0.30	10.00	0.28	0.63	0.91
MIX	2.00	3.20	0.12	0.30	10.00	0.12	1.22	1.34
MIX	1.00	3.20	0.11	0.34	12.53	0.12	1.25	1.37
MIX	0.50	3.20	0.11	0.30	10.00	0.01	1.37	1.38
MIX	0.25	3.20	0.10	0.29	10.00	0.01	1.38	1.39
70110	2.00	1.00	0.11	0.33	10.00	0.78	0.36	1.14
70110	1.00	1.00	0.11	0.34	12.68	0.46	0.43	0.89
70110	0.50	1.00	0.14	0.29	10.00	0.23	0.64	0.87
70110	0.25	1.00	0.10	0.32	10.00	0.21	0.67	0.88
70110	2.00	3.20	0.12	0.33	10.00	0.05	1.46	1.51
70110	1.00	3.20	0.11	0.36	12.95	0.03	0.78	0.81
70110	0.50	3.20	0.10	0.33	10.00	0.00	1.00	1.00
70110	0.25	3.20	0.09	0.31	10.00	0.00	1.57	1.57

average of three measurements were used to determine each colloid concentration (reproducibility was typically within 1% of C_i). The duration of the tracer suspension pulse and the average aqueous Darcy velocity (q) for the various column experiments is also given in Table 1.

Following completion of the transport experiments, the spatial distribution of reversibility retained colloids in the sand was determined. The saturated sand was carefully excavated into 20 ml scintillation vials containing excess 0.001 M NaBr solution. The vials were then slowly shaken for 4 h using an Eberbach shaker (Eberbach Corporation, Ann Arbor, Michigan), and the concentration of colloids in the excess solution was determined. The mass of water and sand in the tubes was determined by weight.

A number balance was conducted at the end the column experiment by normalizing the recovered colloid number in the effluent and sand by the amount injected into the column.

To account for mass balance errors in the experimental data, the measured concentration of colloids retained in the sand was multiplied by $(1-M_E)/M_S$; where M_E and M_S are the measured colloid mass fraction in the effluent and sand, respectively. This approach assumes that the colloid mass balance error occurs primarily on the solid phase.

3. Results and discussion

3.1. Breakthrough curves and spatial distributions

Figs. 1 and 2 present plots of the effluent concentration curves for various input concentrations of 1.0 and 3.2 μm colloids in 3550 (Figs. 1a and 2a), MIX (Figs. 1b and 2b),

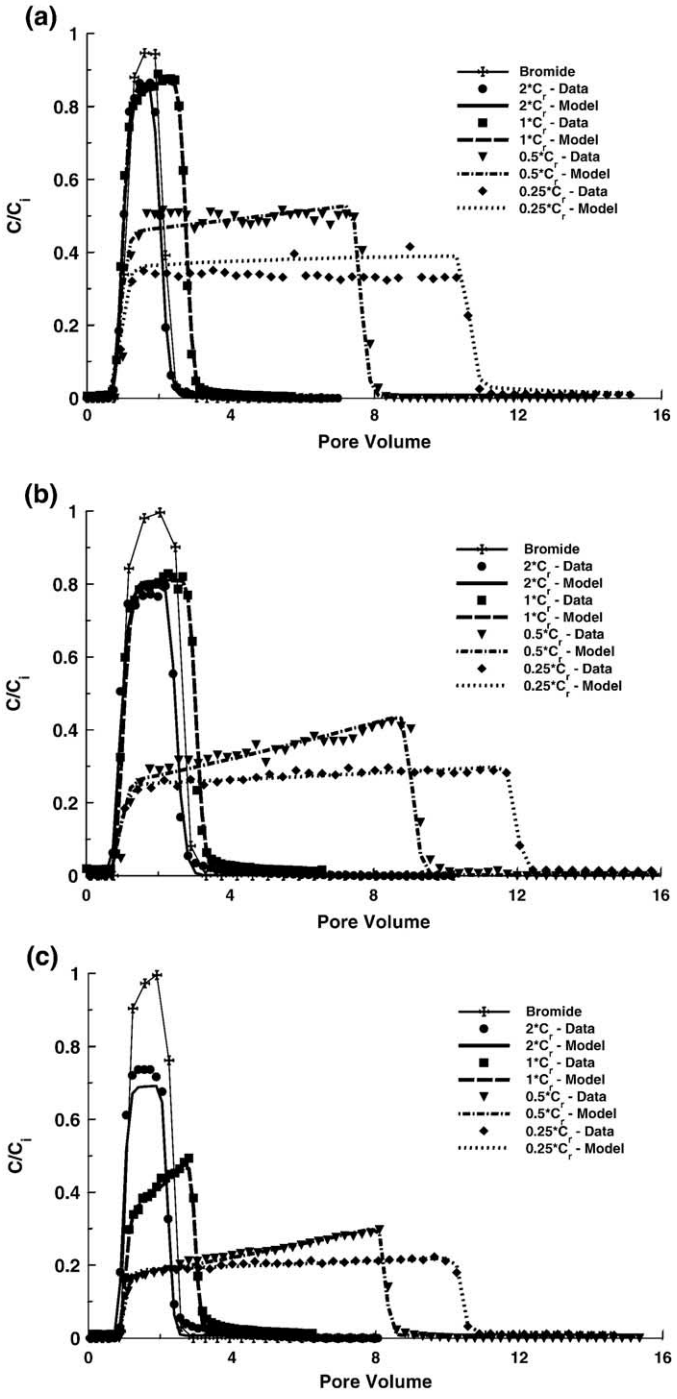

Fig. 1. Plots of observed and simulated effluent concentration curves for various input concentrations ($2*C_r$, C_r, $0.5*C_r$, and $0.25*C_r$) of 1.0 μm colloids in 3550 (a), MIX (b), and 70110 (c) sand. A representative bromide effluent concentration curve is also shown for reference. Simulations considered straining, liberation, attachment, and detachment (Eqs. (1)–(3)). Table 4 provides a summary of predicted (k_{att} and k_{det}) and fitted (k_{str} and k_{lib}) model parameters.

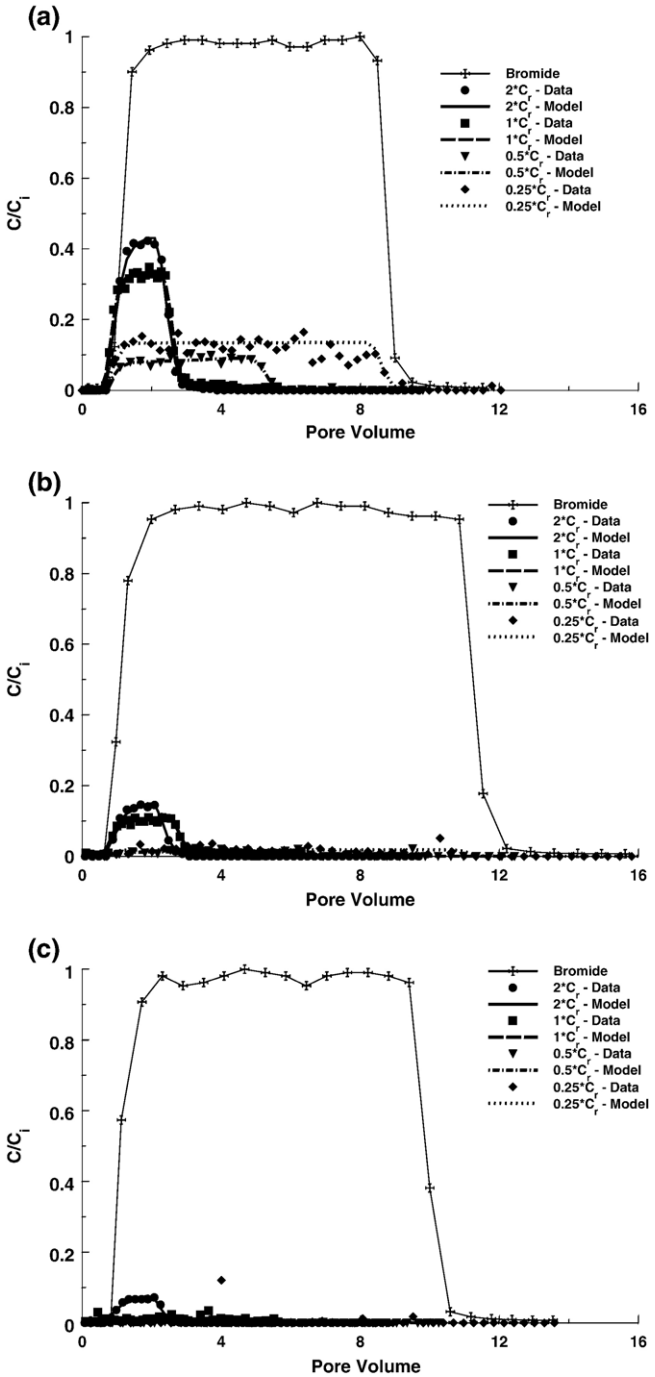

Fig. 2. Plots of observed and simulated effluent concentration curves for various input concentrations ($2 * C_r$, C_r, $0.5 * C_r$, and $0.25 * C_r$) of 3.2 μm colloids in 3550 (a), MIX (b), and 70110 (c) sand. A representative bromide effluent concentration curve is also shown for reference. Simulations considered straining, liberation, attachment, and detachment (Eqs. (1)–(3)). Table 4 provides a summary of predicted (k_{att} and k_{det}) and fitted (k_{str} and k_{lib}) model parameters.

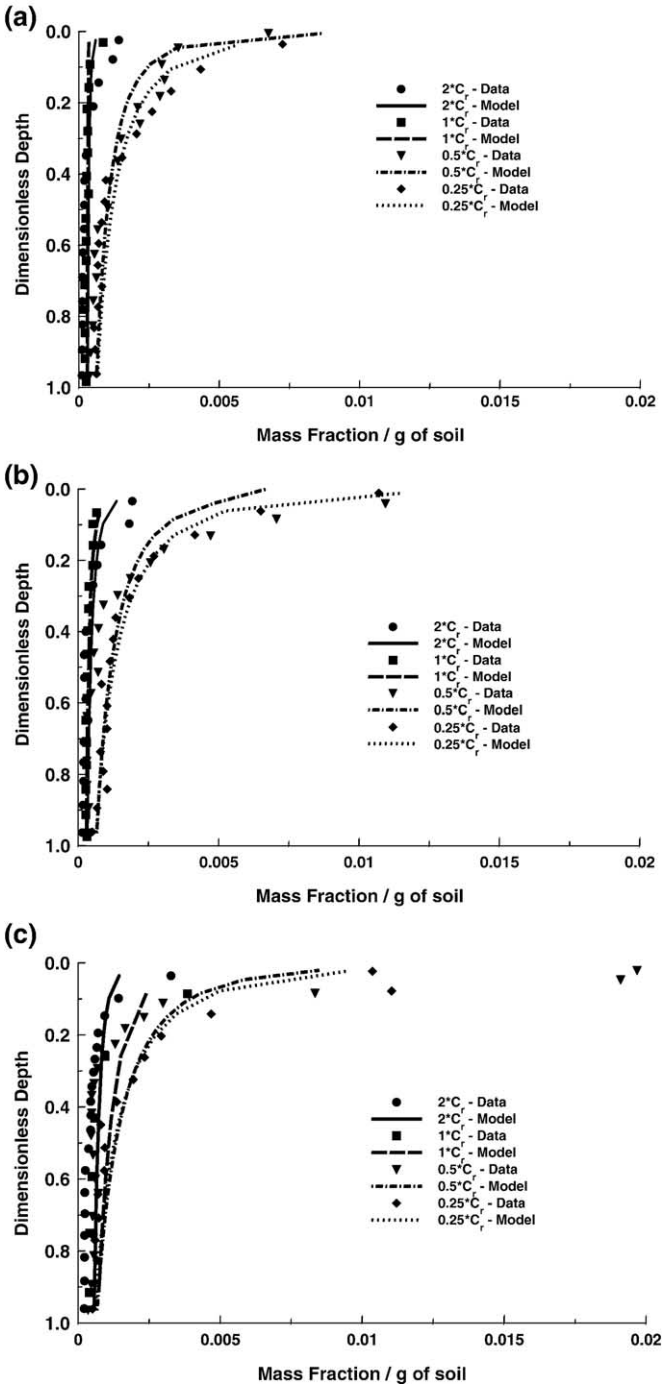

Fig. 3. Plots of observed and simulated spatial distribution of retained colloids for the various input concentrations ($2 * C_r$, C_r, $0.5 * C_r$, and $0.25 * C_r$) of 1.0 μm colloids in 3550 (a), MIX (b), and 70110 (c) sand. Simulations considered straining, liberation, attachment, and detachment (Eqs. (1)–(3)). Table 4 provides a summary of predicted (k_{att} and k_{det}) and fitted (k_{str} and k_{lib}) model parameters.

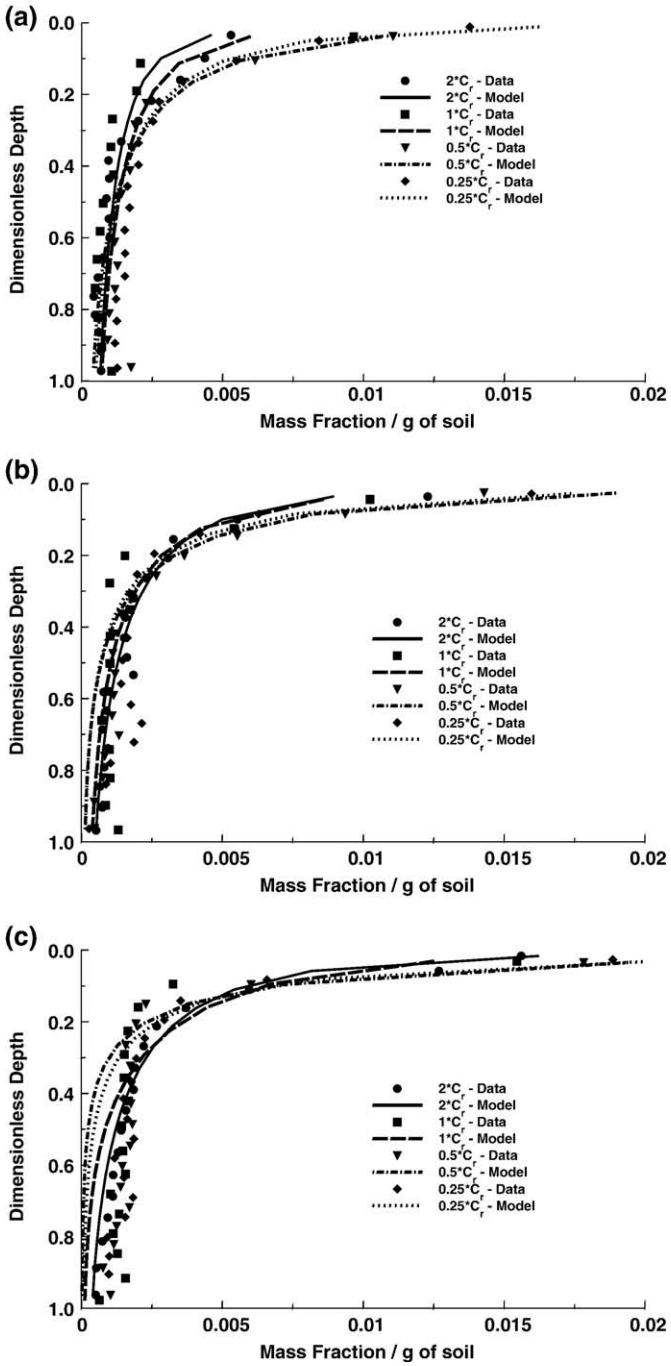

Fig. 4. Plots of observed and simulated spatial distribution of retained colloids for the various input concentrations ($2 * C_r$, C_r, $0.5 * C_r$, and $0.25 * C_r$) of 3.2 μm colloids in 3550 (a), MIX (b), and 70110 (c) sand. Simulations considered straining, liberation, attachment, and detachment (Eqs. (1)–(3)). Table 4 provides a summary of predicted (k_{att} and k_{det}) and fitted (k_{str} and k_{lib}) model parameters.

and 70110 (Figs. 1c and 2c) sands, respectively. The colloid effluent concentrations were normalized to the input colloid concentration, so that concentration dependent differences in the transport behavior could be distinguished. A representative bromide effluent concentration curve was also shown for reference and to demonstrate the uniformity of the aqueous phase flow field. Table 1 provides the recovered effluent, sand, and the total colloid mass fraction (MB_T) for the experimental systems. For a particular sand and colloid, lower input concentrations tended to result in lower peak effluent concentrations and greater colloid mass retention (cf., Fig. 1a and Table 1). For a particular input concentration, decreasing the median grain size (cf., comparison of Fig. 1a, b, and c) or increasing the colloid size (cf., comparison of Figs. 1a and 2a) results in a lower peak effluent concentration and greater mass retention (cf., Table 1). Some of the effluent concentration curves for colloids in Figs. 1 and 2 also exhibited asymmetric breakthrough curves (cf., $0.5*C_r$ in Fig. 1b, and $1*C_r$ and $0.5*C_r$ in Fig. 1c); i.e., during the period of continued colloid addition the effluent concentration increased with time.

Figs. 3 and 4 present plots of the spatial distribution of retained colloids for various input concentrations of 1.0 and 3.2 μm colloids in 3550 (Figs. 3a and 4a), MIX (Figs. 3b and 4b), and 70110 (Figs. 3c and 4c) sands, respectively. Here plots were given as the fraction of total colloid mass per gram of dry sand as a function of normalized (by the column length) distance from the column inlet. Because a similar mass of colloids was added to each column, these plots reflect differences in colloid deposition. Figs. 3 and 4 indicate that the vast majority of colloid mass was retained at or near the column inlet. Consistent with the effluent concentration curves shown in Figs. 1 and 2 and the mass balance information given in Table 1, the mass retention generally increased with decreasing input concentration (cf., Fig. 3a), decreasing sand size (cf., comparison of Fig. 3a, b, and c), and increasing colloid size (cf., comparison of Figs. 3a and 4a).

3.2. Simulations of time-dependent deposition

Numerical simulations were conducted to help identify the mechanisms controlling the transport and deposition behavior in the column experiments. Time dependent colloid deposition (attachment or straining) was considered as a possible explanation for the observed concentration dependent transport behavior (Figs. 1–4). Fig. 5a, b, and c present illustrative plots of observed and simulated (time dependent attachment or straining) effluent concentration curves (Fig. 5a) and spatial distributions (Fig. 5b and c) for various input concentration levels of 1 μm colloids in the 70110 sand. The simulations were obtained by separately fitting time dependent attachment (k_{att}, k_{det}, and S_{att}^{max}) or straining (k_{str} and S_{str}^{max}) model parameters to the effluent concentration curves (Tables 2 and 3). The time dependent attachment (blocking) model provided a reasonable description of the effluent data (Fig. 5a), but a very poor description of the spatial distributions (Fig. 5b). The blocking model under estimated the colloid mass retention at the column inlet and over estimated the attached mass with increasing distance. Conversely, the time dependent straining model provided a reasonable description of both the effluent and spatial distribution data (Fig. 5a and c).

Tables 2 and 3 summarizes the fitted attachment (k_{att}, k_{det}, and $S_{att}^{*max}=S_{att}^{max}/N_i$; where N_i is the number of colloids in a unit volume of C_i) and straining (k_{str} and $S_{str}^{*max}=S_{str}^{max}/N_i$) model parameters, respectively, for all the column experiments. These tables also include statistical measures for the goodness of parameter fits; i.e., standard error (SE) and coefficient of linear regression for effluent (r_e^2) and spatial distribution data (r_s^2). Values of r_e^2 were typically high for both time-dependent attachment and straining models in systems that exhibited effluent concentrations greater than around 5%. Values of r_s^2 for the time-

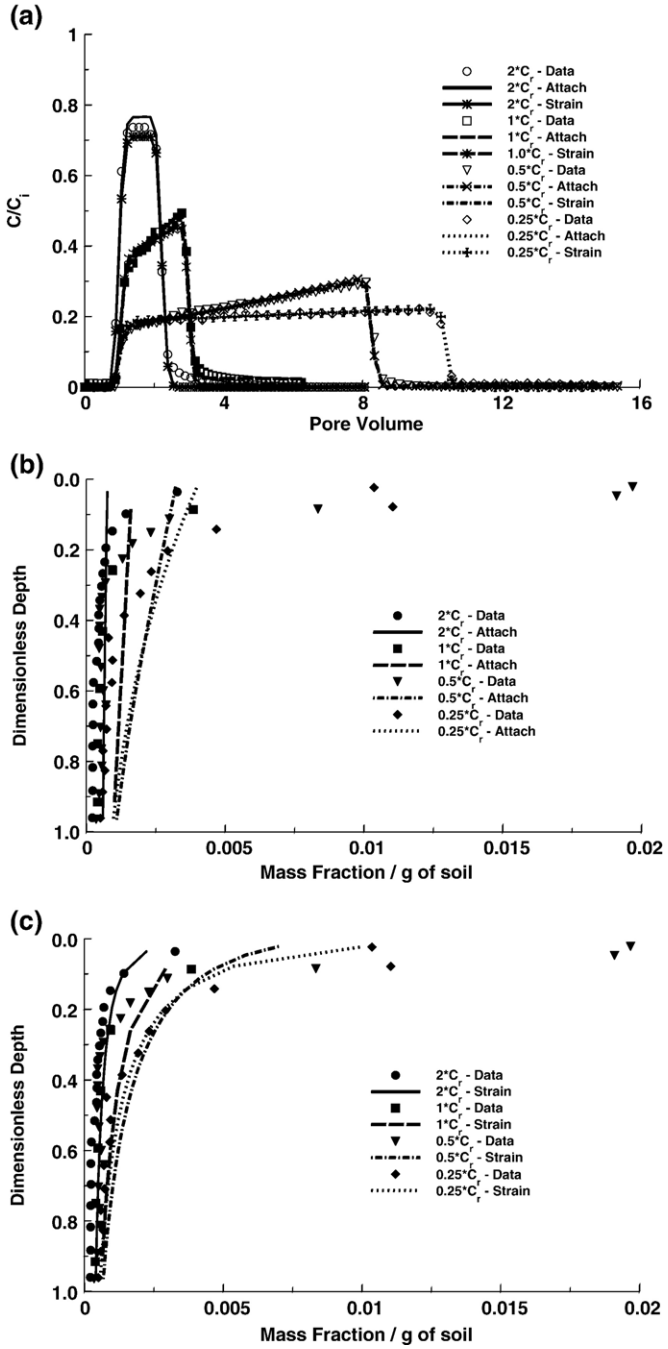

Fig. 5. Plots of observed and simulated (time dependent attachment or straining) effluent concentration curves (a) and spatial distributions ((b) and (c) are for time dependent attachment and straining, respectively) for the various input concentration levels ($2 * C_r$, C_r, $0.5 * C_r$, and $0.25 * C_r$) of 1 μm colloids in the 70110 sand. The simulations were obtained by separately fitting time dependent attachment (k_{att}, k_{det}, and S_{att}^{max}) or straining (k_{str} and S_{str}^{max}) model parameters to the effluent concentration curves. Tables 2 (attachment) and 3 (straining) provide a summary of the fitted model parameters.

Table 2
Fitted time dependent attachment model (Eq. (1)) parameters ($S_{att}^{*max}=S_{att}^{max}/N_i$, k_{att}, and k_{det})

Sand type	C_i/C_r	d_c/d_{50}	S_{att}^{*max} (SE) (N N_i^{-1} g^{-1})	k_{att} (SE) (h^{-1})	k_{det} (SE) (h^{-1})	r_e^2	r_s^2
3550	2.00	0.003	0.3 (7.6)	0.28 (0.07)	0.00 (0.07)	1.00	0.66
3550	1.00	0.003	100.0 (30,222.0)	0.21 (0.02)	0.05 (0.02)	1.00	0.42
3550	0.50	0.003	2.8 (4.3)	2.18 (0.10)	0.01 (0.01)	0.97	0.72
3550	0.25	0.003	100.0 (3789.0)	2.20 (0.58)	0.00 (0.04)	0.99	0.76
3550	2.00	0.009	1.0 (2.6)	2.15 (0.08)	0.00 (0.01)	0.99	0.77
3550	1.00	0.009	100.0 (1672.4)	1.76 (0.04)	0.02 (0.01)	0.99	0.43
3550	0.50	0.009	8.3 (6.5)	4.70 (0.09)	0.00 (0.00)	0.98	0.68
3550	0.25	0.009	100.0 (697.4)	3.13 (0.13)	0.00 (0.01)	0.89	0.69
MIX	2.00	0.004	100.0 (29,110.0)	0.62 (0.06)	0.03 (0.04)	0.99	0.61
MIX	1.00	0.004	4.3 (9.2)	0.34 (0.04)	0.06 (0.03)	0.99	0.71
MIX	0.50	0.004	1.7 (0.1)	4.52 (0.12)	0.01 (0.01)	0.98	0.60
MIX	0.25	0.004	12.7 (1.7)	3.17 (0.03)	0.01 (0.00)	1.00	0.66
MIX	2.00	0.013	2.8 (1.7)	5.18 (0.12)	0.00 (0.01)	0.98	0.66
MIX	1.00	0.013	100.0 (847.8)	3.81 (0.06)	0.02 (0.00)	0.98	0.62
MIX	0.50	0.013	10.3 (10.3)	11.70 (0.71)	0.01 (0.01)	0.57	0.85
MIX	0.25	0.013	100.0 (624.1)	9.51 (0.51)	0.00 (0.01)	0.49	0.71
70110	2.00	0.007	100.0 (101,930.0)	0.54 (0.11)	0.00 (0.06)	1.00	0.47
70110	1.00	0.007	0.6 (0.0)	1.64 (0.02)	0.05 (0.00)	1.00	0.58
70110	0.50	0.007	2.5 (0.2)	5.09 (0.05)	0.00 (0.00)	0.99	0.37
70110	0.25	0.007	17.0 (2.4)	3.10 (0.02)	0.01 (0.00)	1.00	0.71
70110	2.00	0.021	2.0 (3.1)	6.35 (0.17)	0.00 (0.01)	0.96	0.71
70110	1.00	0.021	100.0 (4566.0)	7.11 (0.61)	0.11 (0.03)	0.01	0.47
70110	0.50	0.021	12.7 (32.5)	15.85 (1.63)	0.01 (0.02)	0.17	0.70
70110	0.25	0.021	100.0 (2982.2)	10.61 (2.60)	0.00 (0.03)	0.02	0.73

Straining model (Eqs. (2), (3)) parameters were set equal to zero. Statistical parameters include the standard error (SE), as well as the coefficient of linear regression for effluent (r_e^2) and spatial distribution (r_s^2) data.

dependent attachment model were much lower than the corresponding values for the time-dependent straining model. Lower values of S_{att}^{max} (Table 2) and S_{str}^{max} (Table 3) indicate an increasing time dependence during deposition. Model predictions were relatively insensitive to changes in S_{att}^{max} and S_{str}^{max} for larger values and therefore produced much higher SE. Systematic trends in S_{att}^{max} with input concentration, colloid size, and sand size were not readily apparent (Table 2), because decreasing S_{att}^{max} and k_{att} both produce higher effluent concentrations (nonunique parameter fits). Values of S_{str}^{max} in Table 3 were also subject to similar limitations.

For a given input concentration level, values of the colloid deposition rate coefficient (k_{att} or k_{str}) increased for decreasing sand size and increasing colloid size (Tables 2 and 3). This result is similar to that reported by Bradford et al. (2003). The values of k_{det} in Table 2 were typically several orders of magnitude lower than k_{att}. For a given sand and colloid size, values of k_{att} (Table 2) and k_{str} (Table 3) tended to increase with decreasing input concentration. This result was somewhat surprising since the rate of blocking of attachment sites or filling of straining sites was expected to decrease with decreasing input concentration.

Fig. 6 presents a plot of M_E as a function of d_c/d_{50} for the various input concentration levels; where d_c is the colloid diameter. For a given input concentration, the value of M_E decreased with increasing d_c/d_{50}. For a given d_c/d_{50} value, M_E tended to increase with increasing input concentration, especially for lower values of d_c/d_{50}. Similar results have been reported in the literature (Tan et al., 1994; Liu et al., 1995). Time dependent attachment or straining behavior predicts a constant value of M_E (a fixed number/volume of colloid deposition sites) for a given

Table 3
Fitted time dependent straining model (Eqs. (2) and (3)) parameters ($S_{str}^{*max}=S_{str}^{max}/N_i$ and k_{str})

Sand type	C_i/C_r	d_c/d_{50}	S_{str}^{*max} (SE) (N N_i^{-1} g^{-1})	k_{str} (SE) (h^{-1})	r_e^2	r_s^2
3550	2.00	0.003	100.0 (85505.0)	1.81 (0.3)	1.00	0.93
3550	1.00	0.003	0.1 (0.0)	1.16 (0.4)	1.00	0.82
3550	0.50	0.003	8.4 (29.6)	13.63 (0.6)	0.97	0.91
3550	0.25	0.003	100.0 (337.4)	13.34 (0.6)	0.99	0.99
3550	2.00	0.009	3.1 (13.6)	15.30 (0.7)	0.99	0.93
3550	1.00	0.009	100.0 (990.8)	12.97 (0.3)	0.96	0.87
3550	0.50	0.009	5.8 (0.6)	32.47 (1.3)	0.96	0.95
3550	0.25	0.009	100.0 (345.0)	20.91 (0.8)	0.89	0.99
MIX	2.00	0.004	100.0 (22,429.0)	4.86 (0.6)	0.99	0.99
MIX	1.00	0.004	100.0 (17,250.0)	2.81 (0.3)	0.99	0.99
MIX	0.50	0.004	2.2 (0.2)	36.64 (1.2)	0.98	0.98
MIX	0.25	0.004	15.5 (2.1)	25.05 (0.3)	1.00	1.00
MIX	2.00	0.013	4.3 (8.2)	40.95 (1.0)	0.98	0.97
MIX	1.00	0.013	39.7 (80.8)	32.71 (0.7)	0.98	0.93
MIX	0.50	0.013	15.6 (19.4)	93.45 (5.8)	0.56	0.97
MIX	0.25	0.013	100.0 (250.2)	75.64 (4.0)	0.48	0.97
70110	2.00	0.007	100.0 (17,377.0)	6.79 (0.8)	1.00	0.95
70110	1.00	0.007	1.2 (0.4)	16.00 (1.0)	0.99	0.92
70110	0.50	0.007	3.7 (0.2)	50.35 (0.6)	0.99	0.77
70110	0.25	0.007	23.1 (3.3)	29.57 (0.3)	1.00	0.85
70110	2.00	0.021	2.9 (1.0)	63.98 (1.7)	0.97	0.96
70110	1.00	0.021	100.0 (1706.6)	74.23 (8.0)	0.01	0.92
70110	0.50	0.021	21.9 (40.9)	156.62 (19.8)	0.17	0.97
70110	0.25	0.021	100.0 (786.0)	102.88 (26.3)	0.02	0.99

The value of β was set equal to 0.432 (Bradford et al., 2003). Attachment model parameters were set equal to zero (Eq. (1)). Statistical parameters include the standard error (SE), as well as the coefficient of linear regression for effluent (r_e^2) and spatial distribution (r_s^2) data.

sand and colloid; i.e., only the rate of the deposition is dependent on the input concentration. Hence, time dependent deposition (attachment or straining) behavior cannot account for the observed concentration dependency in Fig. 6.

3.3. Simulations of straining, liberation, attachment, and detachment

Figs. 1–4 also include plots of simulated effluent concentration curves (Figs. 1 and 2) and the spatial distribution data (Figs. 3 and 4) when straining, liberation, attachment, and detachment were modeled according to Eqs. (1)–(3). For simplicity, the values of S_{att}^{max} and S_{str}^{max} were set equal to values large enough to eliminate the time dependent deposition behavior discussed in the previous section. In these simulations the clean-bed attachment coefficient was estimated from the predicted collector efficiency (Rajagopalan and Tien, 1976) and the fitted value of the colloid sticking efficiency for 0.45 μm carboxyl colloids in 3550, MIX, and 70110 sands (Bradford et al., 2002). This colloid size exhibited little straining in these sands (Bradford et al., 2002). The detachment coefficient was also determined from transport experiments for the 0.45 μm colloids (Bradford et al., 2002). The straining and liberation coefficients were fitted to each experimental effluent concentration curve presented in Figs. 1 and 2. Figs. 1–4 indicate that this model provided a reasonable fit to both the effluent concentration curves and the spatial distribution data.

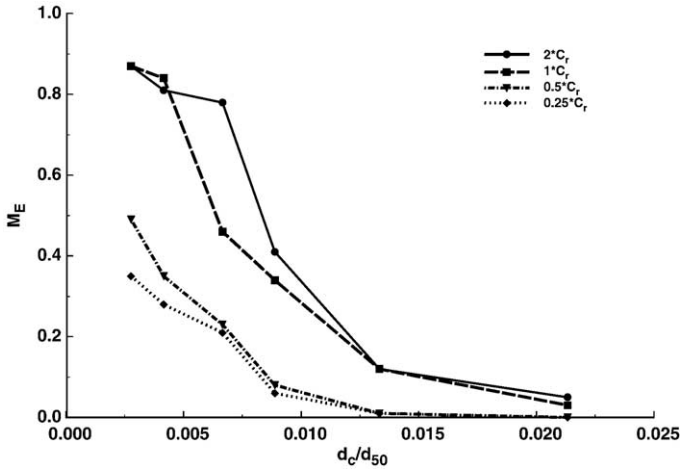

Fig. 6. A plot of the measured M_E (colloid mass fraction recovered in the effluent) as a function of d_c/d_{50} (ratio of colloid to median grain diameters) for the various input concentration levels ($2*C_r$, C_r, $0.5*C_r$, and $0.25*C_r$).

Table 4 summarizes the attachment, detachment, straining, and liberation coefficients for each column experiment, as well as the percentage of mass retained by straining (%MR_{str}). The r_e^2 values were quite high for systems that exhibited effluent concentrations greater than around 5%,

Table 4
Fitted (k_{str} and k_{lib}) and predicted (k_{att}) model parameters

Sand type	C_i/C_r	d_c/d_{50}	k_{att} (h^{-1})	k_{det} (h^{-1})	k_{lib} (SE) (h^{-1})	k_{str} (SE) (h^{-1})	r_e^2	r_s^2	%MS_{str}
3550	2.00	0.003	0.20	0.04	11.90 (16.7)	0.88 (0.6)	1.00	0.94	31.4
3550	1.00	0.003	0.20	0.04	0.03 (15.9)	0.05 (0.1)	1.00	0.66	4.1
3550	0.50	0.003	0.20	0.04	0.97 (0.3)	13.46 (0.6)	0.97	0.89	92.1
3550	0.25	0.003	0.20	0.04	0.00 (0.3)	12.48 (1.2)	0.99	0.99	98.7
3550	2.00	0.009	0.25	0.02	2.89 (1.2)	13.31 (0.6)	0.99	0.92	90.0
3550	1.00	0.009	0.25	0.02	0.00 (0.3)	11.26 (0.3)	0.99	0.85	88.8
3550	0.50	0.009	0.25	0.02	0.59 (0.2)	29.90 (0.6)	0.98	0.97	96.4
3550	0.25	0.009	0.25	0.02	0.00 (0.2)	20.11 (0.7)	0.90	0.99	94.8
MIX	2.00	0.004	0.11	0.06	0.08 (2.6)	3.90 (0.5)	0.99	0.89	85.1
MIX	1.00	0.004	0.11	0.06	0.00 (1.4)	1.88 (0.3)	0.99	0.92	71.2
MIX	0.50	0.004	0.11	0.06	2.78 (0.3)	34.64 (1.0)	0.98	0.82	97.8
MIX	0.25	0.004	0.11	0.06	0.32 (0.0)	24.03 (0.3)	1.00	0.97	97.7
MIX	2.00	0.013	0.12	0.02	6.04 (0.9)	43.90 (0.9)	0.99	0.97	98.4
MIX	1.00	0.013	0.12	0.02	0.21 (0.4)	31.66 (0.7)	0.98	0.93	98.0
MIX	0.50	0.013	0.12	0.02	1.64 (1.3)	91.99 (5.7)	0.56	0.96	99.4
MIX	0.25	0.013	0.12	0.02	0.05 (0.6)	74.68 (4.0)	0.49	0.98	99.4
70110	2.00	0.007	0.48	0.07	0.00 (2.7)	2.70 (0.7)	1.00	0.91	45.5
70110	1.00	0.007	0.48	0.07	3.79 (1.0)	12.04 (1.0)	1.00	0.90	71.9
70110	0.50	0.007	0.48	0.07	2.16 (0.1)	44.23 (0.5)	0.99	0.85	92.8
70110	0.25	0.007	0.48	0.07	0.16 (0.0)	24.89 (0.2)	1.00	0.84	91.0
70110	2.00	0.021	0.46	0.14	7.69 (1.2)	62.79 (1.6)	0.97	0.94	96.8
70110	1.00	0.021	0.46	0.14	9.64 (4.7)	91.91 (13.8)	0.06	0.80	97.1
70110	0.50	0.021	0.46	0.14	1.59 (3.6)	149.03 (16.4)	0.17	0.97	99.3
70110	0.25	0.021	0.46	0.14	0.02 (3.5)	99.33 (26.5)	0.02	0.99	99.1

The value of k_{det} comes from Bradford et al. (2002), whereas the value of β was set equal to 0.432. Statistical parameters include the standard error (SE) as well as the coefficient of linear regression for effluent (r_e^2) and spatial distribution (r_s^2) data. The percentage of colloid mass retained by straining (%MS_{str}) is also presented.

whereas high values of r_s^2 were typically observed in the experiments. Values of $\%MR_{str}$ indicate that straining was the dominant deposition mechanism in these simulations. For a particular input concentration, the value of k_{str} increased with increasing d_c/d_{50}. For a given sand and colloid, the value of k_{str} also tended to increasing with decreasing C_i. Since straining was most significant at lower input concentrations, the following correlation was developed for k_{str} when $C_i = 0.25 * C_r$:

$$k_{str} = 3.32\left(\frac{d_c}{d_{50}}\right)^{1.23}\varepsilon^{-3.46} \qquad r^2 = 0.95 \tag{4}$$

Bradford et al. (2003) previously developed a correlation for $k_{str}=269.7(d_c/d_{50})^{1.42}$ when $C_i = 1.0 * C_r$ and d_c/d_{50} ranged from 0.0006 to 0.0213. Although both correlations have a similar dependence on d_c/d_{50}, Eq. (4) includes an inverse dependence on porosity suggesting that smaller pore spaces promote greater straining. Correlations for k_{str} at the other input

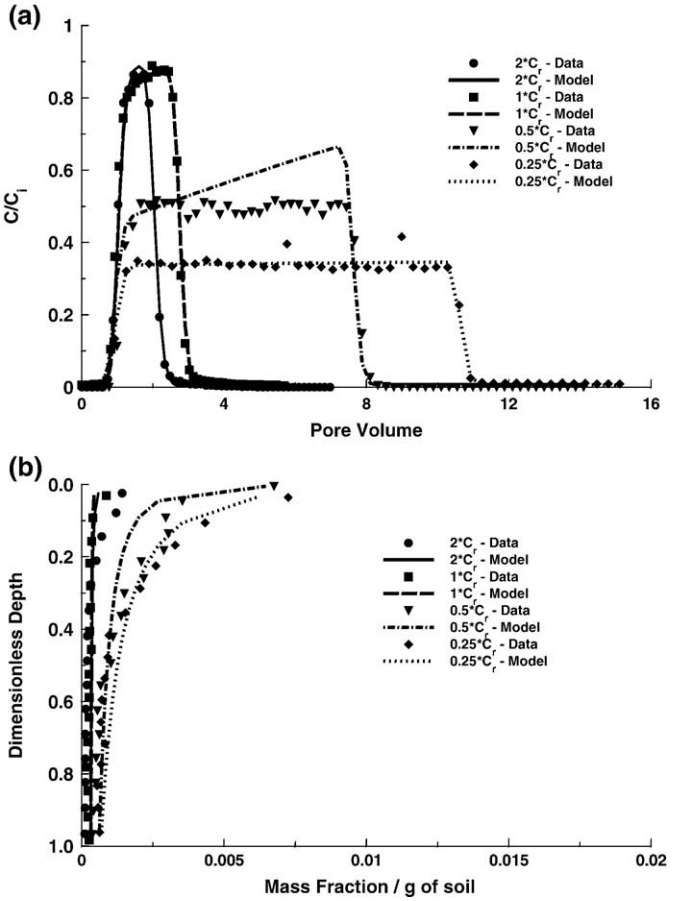

Fig. 7. Observed and simulated (Eqs. (1)–(3)) effluent concentration curves (a) and spatial distributions (b) for various input concentration levels ($2 * C_r$, C_r, $0.5 * C_r$, and $0.25 * C_r$) of 1 μm colloids in 3550 sand. In these simulations, values of k_{str} were obtained from the $C_i = 0.25 * C_r$ data, whereas values of k_{lib} were fitted to each effluent curve. Table 5 provides a summary of predicted (k_{att}, k_{det}, and k_{str}) and fitted (k_{lib}) model parameters.

concentrations ($0.5*C_r$, $1*C_r$, and $2*C_r$) were developed (with $r^2>0.9$) using a functional form similar to Eq. (4). Differences in the these correlations occurred as a result of the concentration dependency of the k_{str}, therefore only Eq. (4) was presented.

Higher values of k_{lib} (Table 4) were used to accounted for the asymmetric shape of some of the effluent concentration curves shown in Figs. 1 and 2, but the concentration dependency was primarily accounted for in these simulations by fitting different values of k_{str} to each set of data. Additional simulations were conducted to better illustrate the potential for the liberation term to account for the observed concentration dependent transport behavior. In these simulations, values of k_{str} and k_{lib} were both fitted to the effluent concentration curves when $C_i=0.25*C_r$. Only k_{lib}, however, was fitted in the simulations for the other input concentration levels ($C_i=0.5*C_r$, $1.0*C_r$, and $2.0*C_r$). In these simulations the value of k_{str} was set equal to $(k_{str}^{ref}v)/v^{ref}$; where v is the pore water velocity and the superscript *ref* indicates the corresponding reference parameters determined in the $C_i=0.25*C_r$ system for a given sand and colloid size. This approach assumes a linear dependence of k_{str} on v as suggested by Foppen et al. (2005). Values for k_{att} and k_{det} were the same as those given in Table 4. Fig. 7a and b present the observed and simulated effluent concentration curves and spatial distributions, respectively, for 1 m colloids in 3550 sand at various input concentration levels according to this modeling approach. These simulations provided a reasonable description of the observed

Table 5
Fitted and/or predicted straining, liberation, attachment, and detachment model parameters

Sand type	C_i/C_r	d_c/d_{50}	k_{att} (h^{-1})	k_{det} (h^{-1})	k_{lib} (SE) (h^{-1})	k_{str} (SE) (h^{-1})	r_e^2	r_s^2	$\%MS_{str}$
3550	2.00	0.003	0.20	0.04	271.21 (1.0)	11.94	1.00	0.93	30.0
3550	1.00	0.003	0.20	0.04	309.81 (1.0)	12.10	0.99	0.78	87.6
3550	0.50	0.003	0.20	0.04	2.99 (11.9)	18.28	0.97	0.89	89.4
3550	0.25	0.003	0.20	0.04	0.01 (0.3)	13.27 (1.1)	0.99	0.99	93.4
3550	2.00	0.009	0.25	0.02	29.67 (5.0)	32.32	0.93	0.92	85.5
3550	1.00	0.009	0.25	0.02	8.93 (22.1)	23.76	0.85	0.81	88.3
3550	0.50	0.009	0.25	0.02	0.11 (307.0)	23.46	0.98	0.96	94.8
3550	0.25	0.009	0.25	0.02	0.00 (0.2)	20.85 (0.7)	0.89	0.99	95.0
MIX	2.00	0.004	0.11	0.06	60.95 (2.0)	27.47	0.92	0.89	86.0
MIX	1.00	0.004	0.11	0.06	169.49 (1.6)	21.83	0.97	0.92	44.4
MIX	0.50	0.004	0.11	0.06	2.92 (11.9)	35.27	0.98	0.82	96.4
MIX	0.25	0.004	0.11	0.06	0.32 (0.0)	24.02 (0.3)	1.00	0.97	97.6
MIX	2.00	0.013	0.12	0.02	34.04 (11.4)	80.29	0.80	0.93	97.9
MIX	1.00	0.013	0.12	0.02	14.56 (55.8)	64.94	0.60	0.84	98.1
MIX	0.50	0.013	0.12	0.02	0.36 (962.9)	73.60	0.56	0.96	99.3
MIX	0.25	0.013	0.12	0.02	0.02 (0.5)	69.22 (3.4)	0.49	0.97	99.3
70110	2.00	0.007	0.48	0.07	339.08 (0.6)	26.52	0.99	0.84	17.5
70110	1.00	0.007	0.48	0.07	13.56 (9.4)	25.74	0.93	0.89	73.2
70110	0.50	0.007	0.48	0.07	1.07 (14.8)	38.42	0.98	0.85	88.3
70110	0.25	0.007	0.48	0.07	0.15 (0.0)	24.87 (0.2)	1.00	0.84	91.1
70110	2.00	0.021	0.46	0.14	44.55 (31.3)	126.54	0.67	0.93	94.5
70110	1.00	0.021	0.46	0.14	14.47 (110.9)	106.33	0.08	0.73	96.4
70110	0.50	0.021	0.46	0.14	0.69 (20121.0)	105.45	0.17	0.95	98.9
70110	0.25	0.021	0.46	0.14	0.04 (3.98)	101.03 (29.5)	0.02	0.99	99.1

Values of k_{str} and k_{lib} were both fitted to the effluent concentration curves when $C_i=0.25*C_r$. However, only k_{lib} was fitted in the simulations for the other input concentration levels ($C_i=0.5*C_r$, $1.0*C_r$, and $2.0*C_r$). The value of k_{str} was set equal to $(k_{str}^{ref}v)/v^{ref}$. Values of k_{att}, k_{det} and β were identical to those given in Table 4. Statistical parameters include the standard error (SE) as well as the coefficient of linear regression for effluent (r_e^2) and spatial distribution (r_s^2) data. The percentage of colloid mass retained by straining ($\%MS_{str}$) is also presented.

concentration dependency in the effluent curves and spatial distributions, suggesting that the liberation term (Eq. (2)) gives one plausible explanation for this behavior.

Table 5 provides the straining, liberation, attachment, and detachment coefficients for each column experiment, when the value of k_{str} for a given sand and colloid size was determined from the $C_i = 0.25 * C_r$ effluent data. The values r_e^2 and r_s^2 were typically high, but sometimes lower than those given in Table 4 because fewer parameters were fitted to the $C_i = 0.5 * C_r$, $1.0 * C_r$, and $2.0 * C_r$ systems (only k_{lib}). In contrast to Table 4, the value of k_{str} was independent of input concentration level and only a function of d_c/d_{50} and ε. The value of k_{lib} tended to increase with increasing C_i. The development of a correlation to quantify and predict the dependence of k_{lib} on C_i was hampered by variability in other system parameters (d_c/d_{50}, ε, v), as well as predicted attachment and detachment. Additional research is therefore needed to predict the dependence of k_{str} and k_{lib} on C_i, as well as on other chemical factors (colloid and porous media surface chemistry, and aqueous phase chemistry). These issues are topics of ongoing research.

References

Bradford, S.A., Yates, S.R., Bettahar, M., Simunek, J., 2002. Physical factors affecting the transport and fate of colloids in saturated porous media. Water Resour. Res. 38 (12), 1327, doi:10.1029/2002WR001340.

Bradford, S.A., Simunek, J., Bettahar, M., Van Genuchten, M.Th., Yates, S.R., 2003. Modeling colloid attachment, straining, and exclusion in saturated porous media. Environ. Sci. Technol. 37 (10), 2242–2250.

Brown, D.G., Stencel, J.R., Jaffe, P.R., 2002. Effects of porous media preparation on bacteria transport through laboratory columns. Water Res. 36, 105–114.

Camesano, T.A., Logan, B.E., 1998. Influence of fluid velocity and cell concentration on the transport of motile and nonmotile bacteria in porous media. Environ. Sci. Technol. 32 (11), 1699–1708.

Camesano, T.A., Unice, K.M., Logan, B.E., 1999. Blocking and ripening of colloids in porous media and their implications for bacterial transport. Colloids Surf., A Physicochem. Eng. Asp. 160 (3), 291–308.

Danielson, R.E., Sutherland, P.L., 1986. In: Klute, A. (Ed.), Porosity, in Methods Soil Analysis: Part 1. Physical and Mineralogical Methods Second Edition, Soil Sci. Soc. Am., Madison, WI.

de Jonge, L.W., Kjaergaard, C., Moldrup, P., 2004. Colloids and colloid-facilitated transport of contaminants in soils: an introduction. Vadose Zone J. 3, 321–325.

Deshpande, P.A., Shonnard, D.R., 1999. Modeling the effects of systematic variation in ionic strength on the attachment kinetics of *Pseudomonas fluorescens* UPER-1 in saturated sand columns. Water Resour. Res. 35 (5), 1619–1627.

Elimelech, M., O'Melia, C.R., 1990. Kinetics of deposition of colloidal particles in porous media. Environ. Sci. Technol. 24 (10), 1528–1536.

Foppen, J.W.A., Mporokoso, A., Schijven, J.F., 2005. Determining straining of *Escherichia coli* from breakthrough curves. J. Contam. Hydrol. 76, 191–210.

Gschwend, P.M., Reynolds, M.D.J., 1987. Monodisperse ferrous phosphate colloids in an anoxic groundwater plume. J. Contam. Hydrol. 1, 309–327.

Herzig, J.P., Leclerc, D.M., Le Golf, P., 1970. Flow of Suspensions Through Porous Media—Application to Deep Infiltration. Flow Through Porous Media. American Chemical Society, Washington, DC, pp. 129–157.

Johnson, P.R., Elimelech, M., 1995. Dynamics of colloid deposition in porous media: blocking based on random sequential adsorption. Langmuir 11 (3), 801–812.

Kim, J.I., 1991. Actinide colloid generation in groundwater. Radiochim. Acta 52/53, 71–81.

Lindqvist, R., Cho, J.S., Enfield, C.G., 1994. A kinetic model for cell density dependent bacterial transport in porous media. Water Resour. Res. 30 (12), 3291–3299.

Liu, D., Johnson, P.R., Elimelech, M., 1995. Colloid deposition dynamics in flow-through porous media: role of electrolyte concentration. Environ. Sci. Technol. 29 (12), 2963–2973.

Logan, B.E., Jewett, D.G., Arnold, R.G., Bouwer, E.J., O'Melia, C.R., 1995. Clarification of clean-bed filtration models. J. Environ. Eng. 121, 869–873.

Marquardt, D.W., 1963. An algorithm for least-squares estimation of nonlinear parameters. J. Soc. Ind. Appl. Math. 11, 431–441.

McCarthy, J.F., Zacchara, J.M., 1989. Subsurface transport of contaminants. Environ. Sci. Technol. 23, 496–502.

McDowell-Boyer, J.M., Hunt, J.R., Sitar, N., 1986. Particle transport through porous media. Water Resour. Res. 22, 1901–1921.

Nyhan, J.W., Brennon, B.J., Abeele, W.V., Wheeler, M.L., Purtymun, W.D., Trujillo, G., Herrera, W.J., Booth, J.W., 1985. Distribution of Plutonium and Americium beneath a 33-yr-old liquid waste disposal site. J. Environ. Qual. 14, 501–509.

Ouyang, Y., Shinde, D., Mansell, R.S., Harris, W., 1996. Colloid-enhanced transport of chemicals in subsurface environments: a review. Crit. Rev. Environ. Sci. Technol. 26, 189–204.

Rajagopalan, R., Tien, C., 1976. Trajectory analysis of deep-bed filtration with the sphere-in-a-cell porous media model. AIChE J. 22, 523–533.

Redman, J.A., Walker, S.L., Elimelech, M., 2004. Bacterial adhesion and transport in porous media: role of the secondary energy minimum. Environ. Sci. Technol. 38, 1777–1785.

Rijnaarts, H.H.M., Norde, W., Bouwer, E.J., Lyklema, J., Zehnder, A.J.B., 1996. Bacterial deposition in porous media related to the clean bed collision efficiency and to substratum blocking by attached cells. Environ. Sci. Technol. 30 (10), 2869–2876.

Rockhold, M.L., Yarwood, R.R., Selker, J.S., 2004. Coupled microbial and transport processes in soils. Vadose Zone J. 3, 368–383.

Ryan, J.N., Gschwend, P.M., 1990. Colloid mobilization in two Atlantic coastal plain aquifers: field studies. Water Resour. Res. 26 (2), 307–322.

Simunek, J., Huang, K., Sejna, M., van Genuchten, M. TH., 1998. The HYDRUS-1D software package for simulating the one-dimensional movement of water, heat, and multiple solutes in variably-saturated media—Version 2.0, IGWMC-TPS-70, International Ground Water Modeling Center, Colorado School of Mines, Golden, Colorado. 186 pp.

Tan, Y., Gannon, J.T., Baveye, P., Alexander, M., 1994. Transport of bacteria in an aquifer sand: experiments and model simulations. Water Resour. Res. 30 (12), 3243–3252.

Tobiason, J.E., O'Melia, C.R., 1988. Physicochemical aspects of particle removal in depth filtration. J. Am. Water Works Assoc. 80, 54–64.

Tufenkji, N., Redman, J.A., Elimelech, M., 2003. Interpreting deposition patterns of microbial particles in laboratory-scale column experiments. Environ. Sci. Technol. 37 (3), 616–623.

Tufenkji, N., Miller, G.F., Ryan, J.N., Harvey, R.W., Elimelech, M., 2004. Transport of *Cryptosporidium* oocysts in porous media: role of straining and physicochemical filtration. Environ. Sci. Technol. 38, 5932–5938.